Experimental and Numerical Study on Concrete Beams Reinforced with Basalt FRP Bars under Static and Impact Loads

Zhijie Huang[1,2], Wensu Chen[1*], Tung T. Tran[1], Thong M. Pham[1], Hong Hao[1*], Zuyu Chen[2], Mohamed Elchalakani[3]

1. Center for Infrastructural Monitoring and Protection, School of Civil and Mechanical Engineering, Curtin University, Australia

2. Institute of Geotechnical Engineering, College of Civil Engineering and Architecture, Zhejiang University, Hangzhou 310058, China

3. School of Civil, Environmental and Mining Engineering, The University of Western Australia, 35 Stirling Highway, WA 6009, Australia

*Corresponding authors. wensu.chen@curtin.edu.au (W. Chen), hong.hao@curtin.edu.au (H. Hao).

Abstract: The application of fiber-reinforced-polymer (FRP) bars to reinforce concrete structures could mitigate the corrosion-induced damage of steel reinforcements. No study has been reported in open literature on flexure-critical or shear-critical concrete beams reinforced with Basalt FRP (BFRP) bars under impact loads. In this study, six concrete beams reinforced with BFRP bars were tested under quasi-static and impact loads. The test results showed the flexure-critical beams experienced the failure mode changing from flexure-governed under quasi-static loads to flexure-shear combined under impact loads. The shear-critical beams still failed in diagonal shear under impact loads, but experienced severer concrete spalling and more critical diagonal cracks on both sides of the beams. The impact performance of concrete beams with higher strength concrete may not be necessarily superior to that of beams with normal strength concrete due to the increased brittleness. Moreover, a numerical model of the tested beams under impact loads was developed and calibrated in LS-DYNA. Numerical results showed increasing tension reinforcement ratio could change the failure mode from flexure-governed to flexure-shear combined along with the reduced maximum midspan deflection. The concrete beams reinforced with BFRP bars had comparable impact resistant performance with the conventional steel reinforced concrete beams.

Keywords: BFRP bars; Concrete beams; Flexure-critical; Shear-critical; Impact loads; Numerical simulation.

1. Introduction

Steel corrosion could reduce the strength and stiffness of steel reinforcements, which undermines the long-term performance of steel reinforced concrete (RC) structures such as strength, deformational behaviour, and durability [1]. Even worse, it could cause catastrophic structural collapse in extreme events. Therefore, monitoring and retrofitting the corrosion damaged RC structures are essential and lead to an increasing lifecycle maintenance cost of steel reinforced structures, especially those in aggressive environments. Owing to the advantages of high tensile strength, lightweight, good corrosion resistance, and fatigue endurance [2], fiber-reinforced-polymer (FRP) reinforcements become a popular replacement for steel reinforcements in concrete structures. In the past decade, many efforts have been made to study the behaviour of concrete beams reinforced with FRP bars under static loads [3-12]. The standards and guides such as CSA S806-12 [13] and ACI 440.1R-15 [14] were also developed to design concrete beams reinforced with FRP bars.

In recent years, dynamic performance of concrete structures under impact loads has drawn much attention due to the extreme events such as accidental explosion, object falling, vehicle collision and terrorist attacks. Many studies have been conducted on concrete beams reinforced with steel bars under impact loads [15-26]. Based on the flexural-shear capacity ratio of concrete beams, these beams were mainly sorted into two types, i.e., flexure-critical beams (also called flexural-failure-type beams [15], with their flexural-shear capacity ratios less than 1 and failed in flexure under static loads) and shear-critical beams (also called shear-failure-type beams [16], with their flexural-shear capacity ratios greater than 1 and failed in shear under static loads). The flexure-critical beams and shear-critical beams had different failure modes with increasing impact velocity. **Fig. 1** illustrates the schematic diagrams of critical cracks and failure modes of these two types of beams with increasing impact velocity, which are based on the results from references [16, 17, 19-21, 26-31]. The flexure-critical beams failed in flexure under static tests and low-velocity impact. As the impact velocity increased, the failure mode of the beams changed to flexure-shear combined or shear-governed. Under high impact velocity, the beams failed in a punching shear-governed mode with shear plug at an angle of approximately 45° initiated from the impact point to the bottom of beams. For shear-critical beams, they failed in shear under static loads and impact loads with low impact velocity. With increasing impact velocity, the beams were prone to fail in combined shear-punching shear mode. Punching shear damage was evident under the impact force profile with high magnitude and short duration induced by high impact velocity [21, 24]. FRP reinforcements and steel reinforcements have different mechanical properties, e.g., the behaviour of FRP reinforcements is linear-elastic, brittle, and strong in tension but relatively weak in compression and shear [32], whereas steel reinforcements behave in an elastic-plastic and ductile manner, and have the same strength in tension and compression. Therefore, the performance of concrete beams reinforced with FRP bars might be different from that of concrete beams reinforced with steel bars under impact loads, which is worthy of studying.

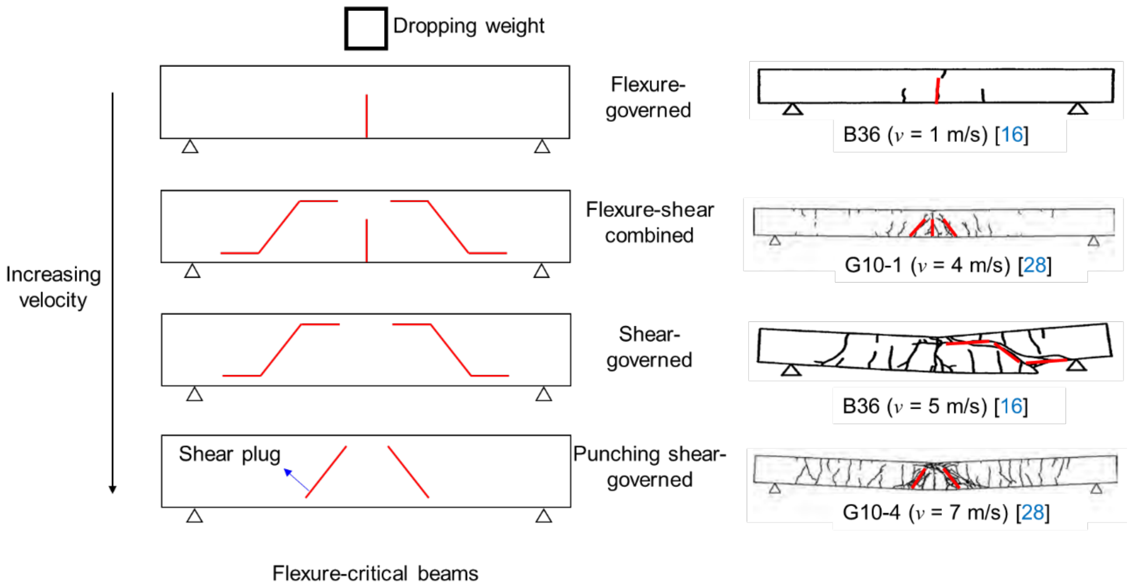

(a)

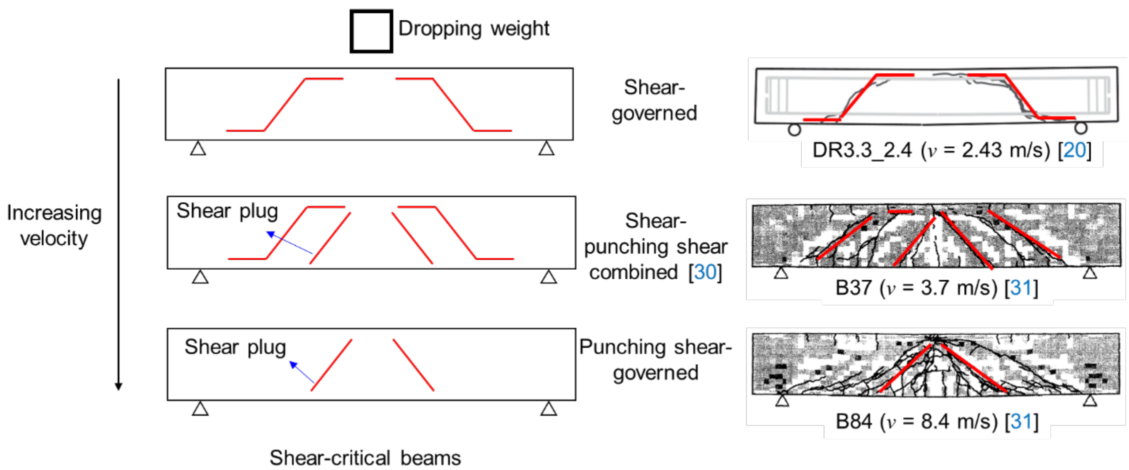

(b)

Fig. 1. Critical cracks and failure modes of (a) flexure-critical beams [16, 28] and (b) shear-critical beams [20, 30, 31] with increasing impact velocity

In the open literature, there are limited studies reporting the performance of flexure-critical concrete beams reinforced with Glass FRP (GFRP) bars under impact loads [33-37]. The test results showed that the beams experienced an average 15% enhancement of moment capacities under impact loads (with the drop mass 110 kg and height 1.2 m) as compared to that under static loads [33]. Reducing stirrup spacing could mitigate the damage level of the beams with lower residual midspan deflection and higher post-impact residual load-carrying capacity [36, 37]. It is worth noting that the performance of concrete beams reinforced with FRP bars under impact loads is influenced by many factors, e.g., concrete material properties, types of FRP bars, longitudinal and transverse reinforcement ratios (related to types of beams, e.g., flexure-critical and shear-critical beams), impact velocity (or drop height), strain rate effect, drop weight, shape of drop hammer, and boundary condition. Although there were limited studies on the impact performance of flexure-critical concrete beams reinforced with GFRP bars, no study can be found on the performance of shear-critical concrete beams reinforced with FRP bars under impact loads yet. In addition, neither flexure-critical nor shear-critical concrete beams reinforced with Basalt FRP (BFRP) bars under impact loads have been reported in open literature. Since BFRP bars had higher tensile strength and modulus of elasticity than GFRP bars [38, 39], the beams reinforced with BFRP bars and GFPR bars may behave differently under impact loads. Therefore, further study on the impact performance of flexure-critical and shear-critical concrete beams reinforced with BFRP bars is deemed essential. It should be noted that the investigations presented in this study is a part of a project which focuses on the structural performance of normal concrete (Ordinary Portland cement Concrete, also called OPC) vs GeoPolymer Concrete (GPC) beams reinforced with BFRP bars. The studies on flexural and shear behaviour of ambient cured GPC concrete beams reinforced with BFRP bars under static and impact loads [40, 41] have been carried out recently. Since GPC and OPC have different material properties, i.e., GPC is more brittle than OPC [42, 43], it is worth studying and reporting the behaviour of flexure-critical and shear-critical OPC beams reinforced with BFRP bars under static and impact loads and comparing the performance between GPC beams and OPC beams.

In this study, three flexure-critical and three shear-critical concrete beams reinforced with BFRP bars were prepared. One flexure-critical beam and one shear-critical beam as reference beams were tested under quasi-static loads whilst four beams with varying concrete strength were tested under impact loads. The effect of compressive strength of concrete on the impact performance of the beams was experimentally investigated. The responses of the beams under quasi-static and impact loads were recorded and analysed in terms of failure mode, crack pattern, midspan deflection, impact forces, and reinforcement strain. Moreover, numerical model was built in LS-DYNA and calibrated against the impact test results. The influence of tension reinforcement ratio and reinforcements material on the impact performance of the beams was further numerically investigated.

2. Experimental details

2.1. Materials

In this study, commercial concrete with the compressive strength of 67 MPa was used for four beams. In order to investigate the effect of the compressive strength of concrete on the impact performance of the beams, other two beams were cast separately with the compressive strength of 44 MPa and 52 MPa. The BFRP bars used in this study are shown in **Fig. 2**. The ultimate tensile strength f_{fu}, elastic modulus E_f, and elongation ε_{fu} provided by the manufacturer [44] were 1200 MPa, 55 GPa, and 2%, respectively.

Fig. 2. BFRP rebars and stirrups

2.2. Details of beam specimens

A total of six beams were prepared and cast, which were divided into two groups, namely, flexure-critical beams and shear-critical beams, based on their flexural-shear capacity ratios. For each group, one beam was tested under static loads as a reference and two beams were prepared for impact tests.

The width (b), height (h), and total length (L_t) of the beams were respectively 150 mm, 200 mm, and 1250 mm, as shown in **Fig. 3**. The flexure-critical beams were longitudinally reinforced with four 10 mm-diameter BFRP bars and transversely reinforced with 10 mm-diameter BFRP stirrups at 100 mm spacing while the shear-critical beams were longitudinally reinforced with four 16 mm-diameter BFRP bars and transversely reinforced with 4 mm-diameter BFRP stirrups at 100 mm spacing. ACI 440.1R-15 [14] was adopted for the design in this study. **Table 1** gives the details of the tested beams. For easy reference, the terminology of the beams consists of four parts: the first part is the concrete type, i.e., OPC; the second part with the letters of 'S' and 'I' means the loading conditions, namely static loads and impact loads, respectively; the third part with the letters of 'FL' and 'SH' represents the types of the beams, namely flexure-critical and shear-critical; the last number denotes the compressive strength f_c' of concrete. For example, Beam OPC-I-SH-67 means the shear-critical beam with the concrete strength of 67 MPa was tested under impact loads.

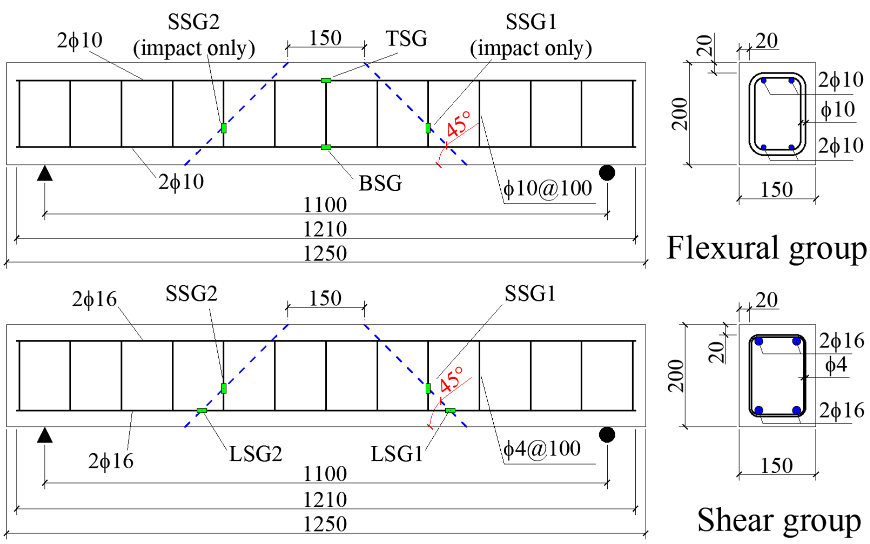

Fig. 3. Configuration of the tested beams and locations of strain gauges

Table 1 Details of the tested beams

Beam group	Beam name	Loading condition	Concrete strength f_c' (MPa)	Tension reinforcement ratio ρ_f (%)	Stirrup ratio ρ_{fv} (%)	Designed flexural capacity (kN) [14]	Designed shear capacity (kN) [14]	Designed flexural-shear capacity ratio
Flexural	OPC-S-FL-67	Static	67	0.63	1.05	80.7	134.5	0.6

Flexural	OPC-I-FL-67	Impact	67	0.63	1.05	80.7	134.5	0.6
Flexural	OPC-I-FL-44	Impact	44	0.63	1.05	67.6	132.3	0.5
Shear	OPC-S-SH-67	Static	67	1.60	0.17	123.0	50.3	2.4
Shear	OPC-I-SH-67	Impact	67	1.60	0.17	123.0	50.3	2.4
Shear	OPC-I-SH-52	Impact	52	1.60	0.17	107.8	48.1	2.2

2.3. Instrumentation

2.3.1 Quasi-static test setup

Fig. 4 shows the quasi-static test setup with three-point bending configuration. The beam was simply supported by a pin and a roller, with a clear span (*L*) of 1,100 mm. The load was applied onto the midspan of the beams using a hydraulic jack at a loading rate of 3 mm/min. A load cell and linear variable differential transformers (LVDT) were used to record the applied load and the midspan deflection, respectively. Two strain gauges (SGs) in the flexure-critical beams, i.e. top strain gauge (TSG) and bottom strain gauge (BSG), and four strain gauges in the shear-critical beams, i.e. longitudinal-bar strain gauges (LSG1 and LSG2) and stirrup strain gauge (SSG1 and SSG2), were bonded onto the reinforcements to capture their strain values as shown in **Fig. 3**. The static results in terms of failure mode, peak load, load-midspan deflection curve, and load-strain curve of reinforcements were analysed.

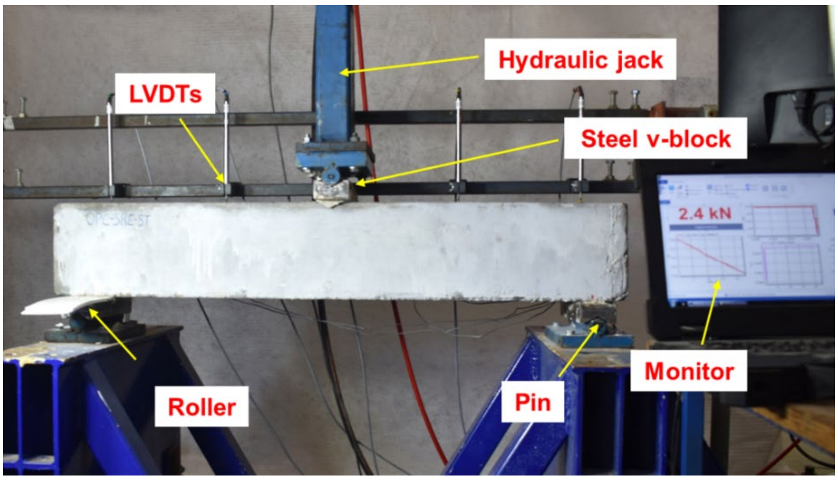

Fig. 4. Quasi-static test setup

2.3.2 Impact test setup

Drop hammer test setup was employed for impact tests as shown in **Fig. 5**. Similar to quasi-static test setup, the beams were simply supported on two steel plates over a pin and a roller with a clear span (*L*) of 1,100 mm. The impact force was recorded by a load cell, which was attached to a load cell adaptor (the size 150 mm × 200 mm × 20 mm) and placed on top of the beam at midspan. To obtain an even contact surface, plaster was utilized between the tested beams and the load cell adaptor. Four strain gauges (i.e., TSG, BSG, SSG1, and SSG2 in the flexure-critical beams, LSG1, LSG2, SSG1, and SSG2 in the shear-critical beams) were attached to the longitudinal bars and stirrups as shown in **Fig. 3**. The 203.5 kg hammer was dropped from a height of 2 m in all tests. More details about the impact test setup can refer to [23]. The actual impact velocity of the drop hammer, midspan deflection, and failure progress of the beams were captured by a high-speed camera with the rate of 20,000 frames per second. A data acquisition system with the sampling rate of 50 kHz was used to collect the data of impact force and reinforcements strain. The results of the impact tests in terms of crack pattern, failure mode, impact force, and reinforcements strain were examined and discussed.

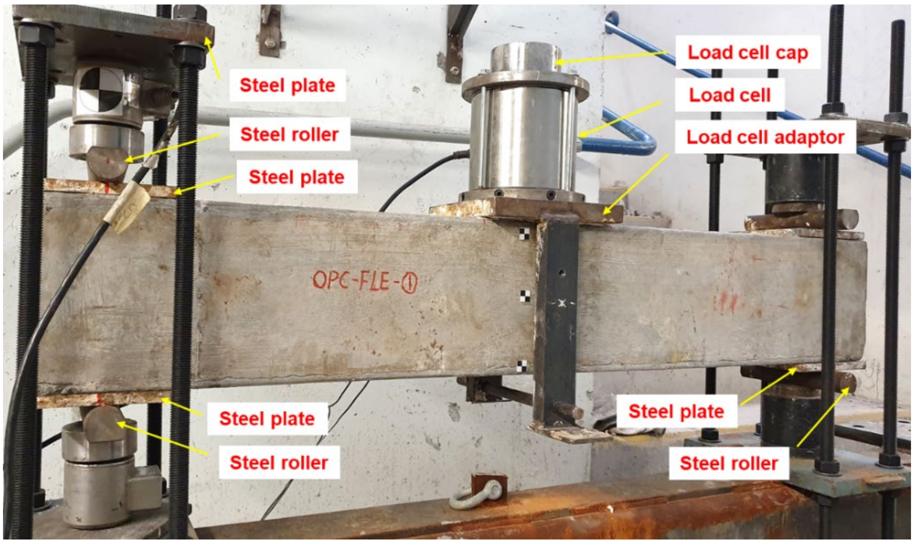

Fig. 5. Impact test setup

3. Quasi-static test results

3.1. Failure modes and crack patterns

The failure modes and crack patterns of Beams OPC-S-FL-67 and OPC-S-SH-67 under quasi-static loads are shown in **Fig. 6**. As shown, Beam OPC-S-FL-67 experienced a flexure-governed failure mode with concrete crushing on the top surface of the beam as expected. The flexural cracks were observed initially at the midspan of the beam, followed by some flexure-shear and shear cracks in the shear span zone. Beam OPC-S-SH-67 failed in diagonal shear, characterized by a wide critical diagonal crack on the right side of the beam initiated from the load point to the supports. A flexural crack appeared at midspan when the applied load increased to 30 kN, followed by a flexural crack on the left side of the beam at about 40 kN as circled in **Fig. 6**. It extended to become flexure-shear crack at around 43 kN. A new flexural crack occurred on the right side of the beam at 46 kN. After that, some new flexural and shear cracks appeared and the existing flexural and shear cracks extended until the failure of the beam. Both beams behaved as expected according to the design.

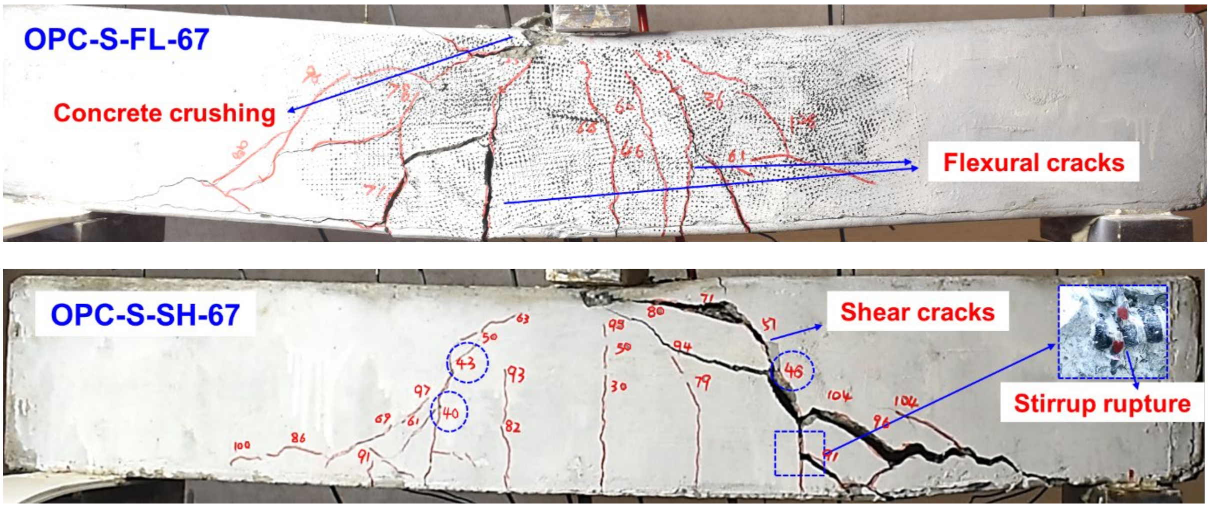

Fig. 6. Failure modes and crack propagation of the two beams under quasi-static loads

3.2. Quasi-static responses

Table 2 summarises the quasi-static test results and **Fig. 7** shows the load-midspan deflection curves of Beams OPC-S-FL-67 and OPC-S-SH-67. It can be seen that both curves are nearly bilinear up to the peak loads, which cover the uncracked stage and the post-cracking stage. The uncracked stage has a relatively steep slope, whereas the post-cracking stage has a reduced slope due to the flexural and shear cracks. The concrete cracking of Beam OPC-S-FL-67 occurred at 30.8 kN. The concrete cover was crushed at 109.1 kN due to the compressive strain of concrete cover reaching the maximum usable strain (assumed to be 0.003 in ACI 440.1R-15 [14], corresponding to the designed flexural capacity of 80.7 kN as listed in **Table 1**). Therefore, the ratio of the designed flexural capacity based on ACI 440.1R-15 [14] to the test value is calculated as 0.74 (i.e. 80.7 kN /109.1 kN), which is close to the reported average values, i.e., 0.73 in [45] and 0.78 in [6]. It is of interest to note that Beam OPC-S-FL-67 could still carry further load up to the peak load (i.e. 112.4 kN) after the concrete cover crushed, which has also been reported in [33, 34, 45, 46].

The concrete cracking of Beam OPC-S-SH-67 was observed at 28.2 kN from its load-midspan curve. It was close to the cracking load of Beam OPC-S-FL-67 (30.8 kN), since the concrete cracking load of the beams was determined by the tensile strength of concrete. The load-midspan deflection curve then gradually increased to the peak load of 106.4 kN, while the designed value was 50.3 kN as listed in **Table 1**. Thus, according to ACI 440.1R-15 [14], the ratio of designed shear capacity to the test value is 0.47 (i.e. 50.3 kN /106.4 kN), which is also close to the reported average values, i.e., 0.52 in [4, 47] and 0.53 in [48]. The midspan deflection of Beam OPC-S-SH-67 at the peak load was 9.2 mm while that of Beam OPC-S-FL-67 was 22.8 mm, indicating that Beam OPC-S-SH-67 failed in a more brittle manner (shear failure) as compared to Beam OPC-S-FL-67 (flexural failure). In general, the test results in the present study indicated that ACI-440.1R-15 [14] significantly underestimated the flexural and shear capacities of concrete beams reinforced with BFRP bars.

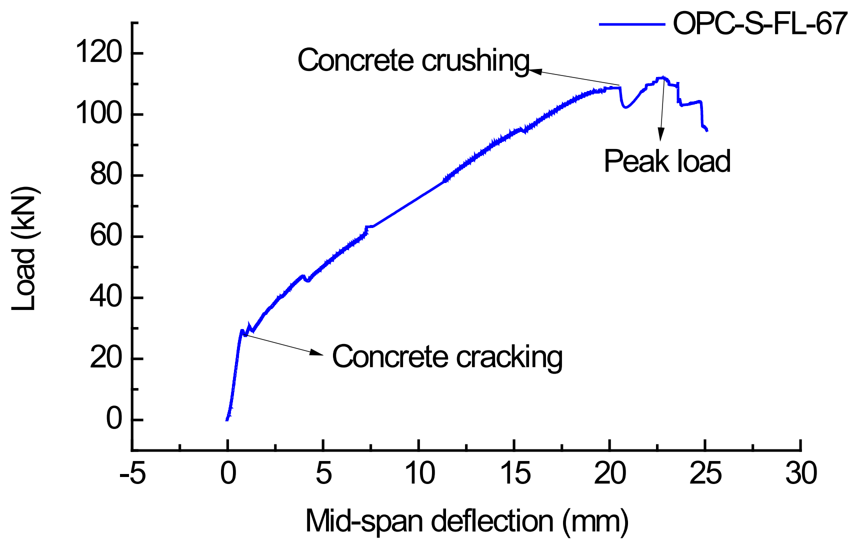

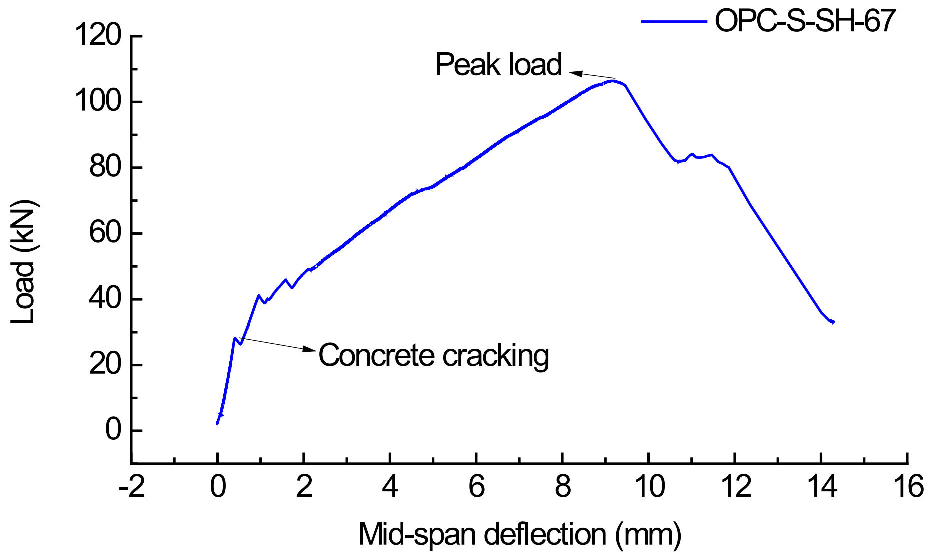

Fig. 7. Load-midspan deflection curves of the two tested beams

Table 2 Quasi-static test results

Beam	OPC-S-FL-67	OPC-S-SH-67
Cracking load (kN)	30.8	28.2
Peak load (kN)	112.4	106.4
Midspan deflection at peak load (mm)	22.8	9.2
Strain at peak load (με)	Not recorded due to strain gauge malfunction	4,981 (LSG1), 7,695 (LSG2) 9,513 (SSG1), 10,170 (SSG2)

Fig. 8 shows the load-strain curves of reinforcements of Beams OPC-S-FL-67 and OPC-S-SH-67. The data of TSG in Beam OPC-S-FL-67 was not properly recorded therefore is not presented herein. It can be seen that all the load-strain curves are approximately bilinear, which are similar to the load-midspan deflection curves of the beams until the peak load as shown in **Fig. 7**. Before concrete cracking (at about 30 kN), the strain of reinforcements (BSG) of Beam OPC-S-FL-67 was very small so that the applied load was mainly sustained by tensile strength of concrete. After a crack occurred at midspan, the load-strain curve of BSG in Beam OPC-S-FL-67 significantly increased. Unfortunately, the strain gauge failed before the applied load reached the peak load of the beam and therefore the strain at peak load was not recorded. Similarly, the longitudinal reinforcement strain (blue lines, LSG1 and LSG2) of Beam OPC-S-SH-67 was also very small before flexural cracks appeared. The strain suddenly increased to 600 με with the occurrence of flexural cracks since the tensile force carried by the concrete material transferred to the tension reinforcements. Subsequently, the load-strain curve gradually increased to the peak load of the beam. The stirrup strain (red lines, SSG1 and SSG2) was also very small at the beginning and then increased rapidly after shear cracks appeared, until the peak load of the beam. The strain of stirrups at peak load was larger than that of tension reinforcements, indicating that the beam eventually failed in shear.

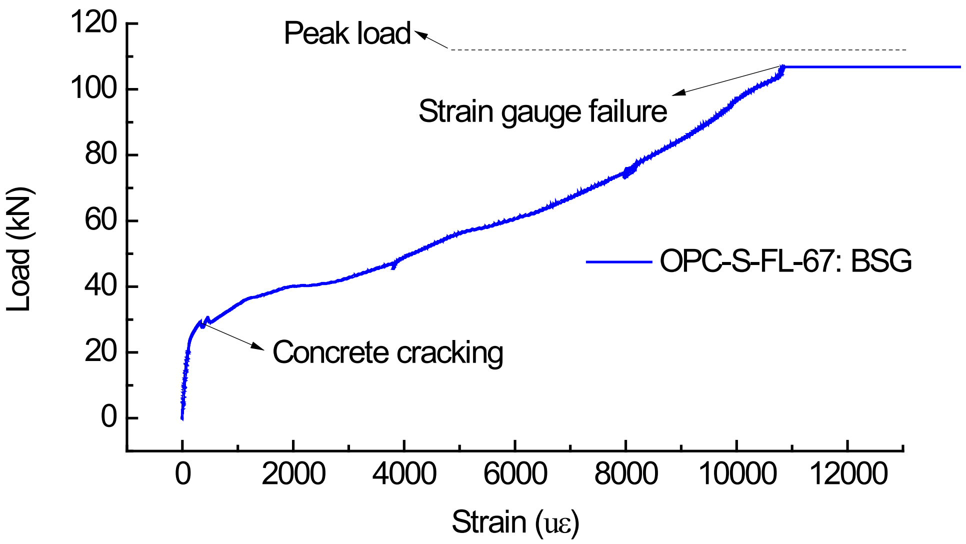

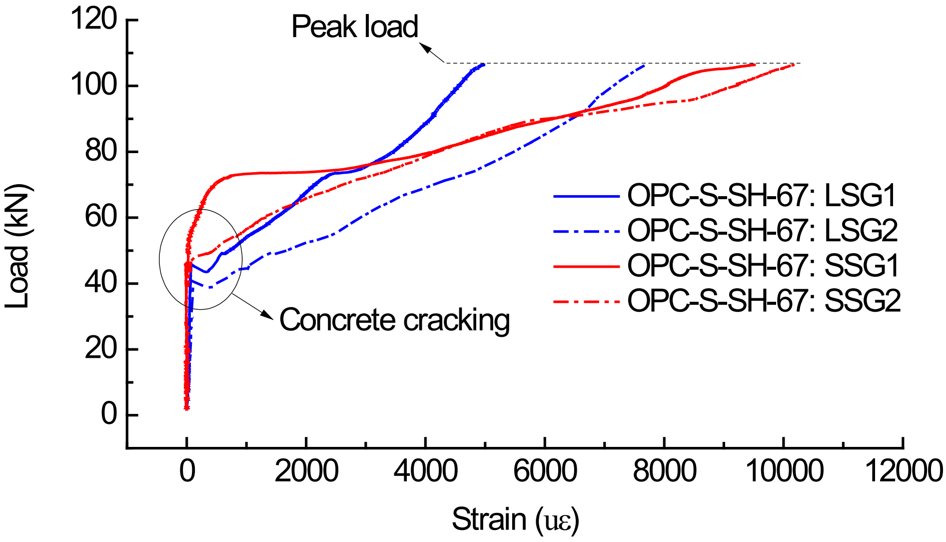

Fig. 8. Load-strain curves of longitudinal reinforcements and stirrups

4. Impact test results

4.1. Failure modes and crack patterns

Fig. 9 shows the failure modes and crack patterns of the four beams tested under impact loads. It can be found that Beams OPC-I-FL-44 and OPC-I-FL-67 failed in a flexure-shear combined mode with critical flexural, flexure-shear, and shear cracks. Concrete crushing on the top and concrete spalling at the bottom were observed on both beams. As compared to Beam OPC-I-FL-44, Beam OPC-I-FL-67 had wider flexural cracks at midspan and larger post-impact residual deformation. Beams OPC-I-SH-52 and OPC-I-SH-67 failed in diagonal shear, characterized by three and two critical diagonal cracks on both sides of the two beams, respectively. Stirrup rupture was observed in both the beams. Beam OPC-I-SH-67 had severer splitting damage of compression BFRP bars and larger post-impact residual deformation at midspan (shown in **Fig. 10**) as compared to Beam OPC-I-SH-52. Thus, the test results showed that higher strength concrete was not necessarily beneficial to the impact performance of concrete beams reinforced with BFRP bars as compared to normal strength concrete, as it could lead to larger maximum and residual deflection of the beams (shown in **Fig. 10**) and severer splitting damage of compression BFRP bars for shear-critical beams. Similar results that reinforced concrete plates with higher strength concrete suffered a higher level of concrete damage under impact loads as compared to those with normal strength concrete were also reported in [49, 50] due to the increased brittleness associated with the increase of concrete strength [49-51]. Generally, the flexure-critical beams experienced the failure mode changing from flexure-governed under quasi-static loads to flexure-shear combined under impact loads, along with severer local damage such as concrete crushing on the top and spalling at the bottom. The shear-critical beams still failed in diagonal shear under impact loads, but experienced severer concrete spalling and more critical diagonal cracks on both sides of the beams as well as wider distribution area of cracks, as compared to Beam OPC-S-SH-67 under quasi-static loads.

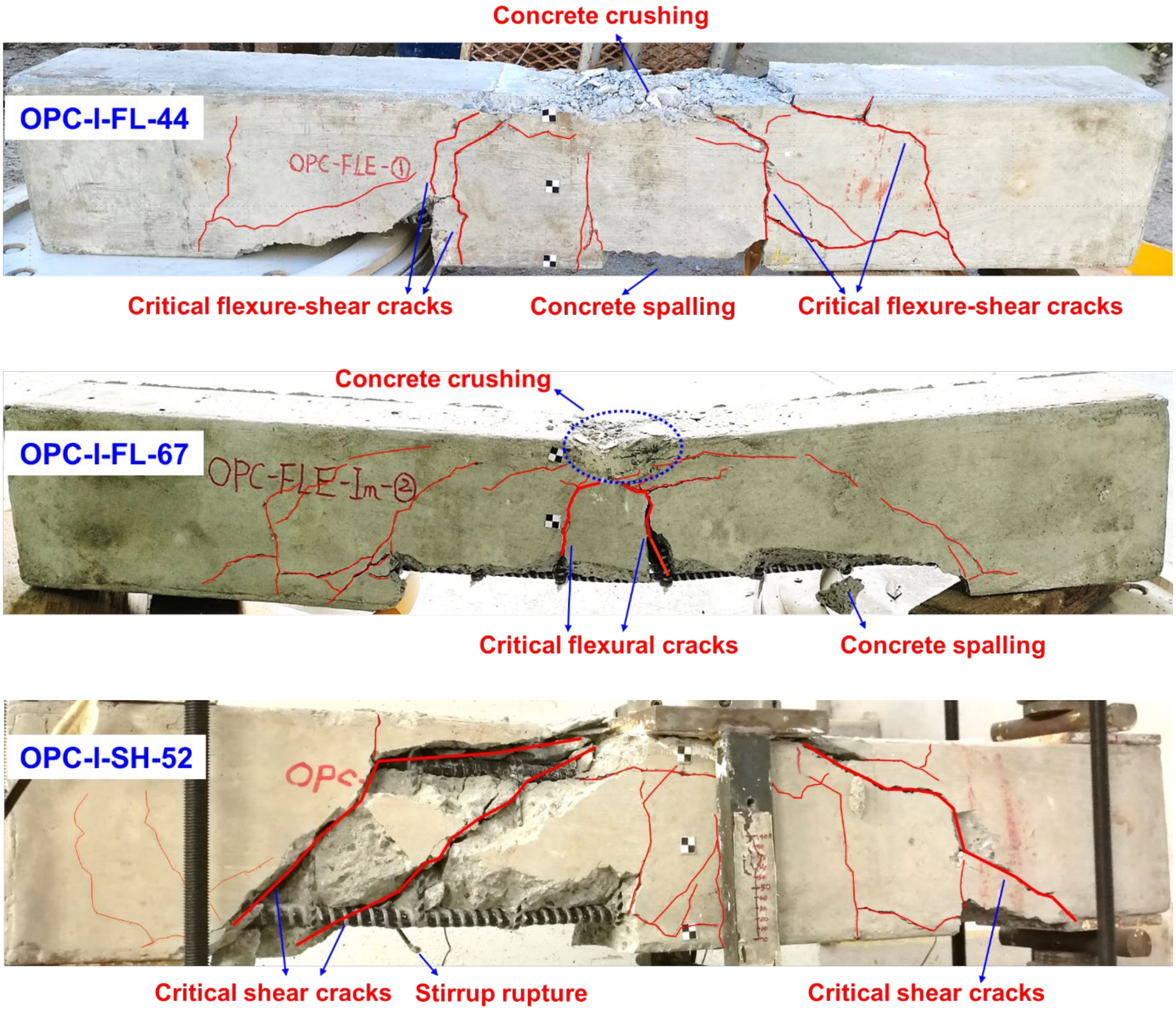

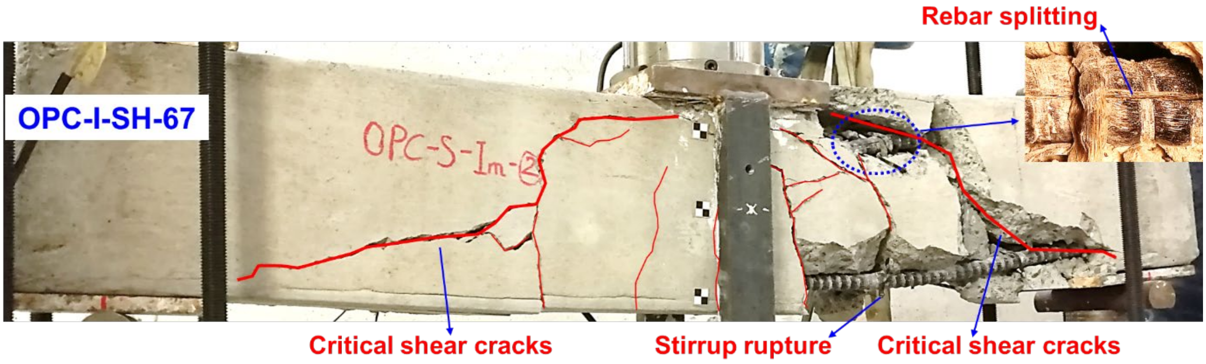

Fig. 9. Failure modes of the tested beams under impact loads

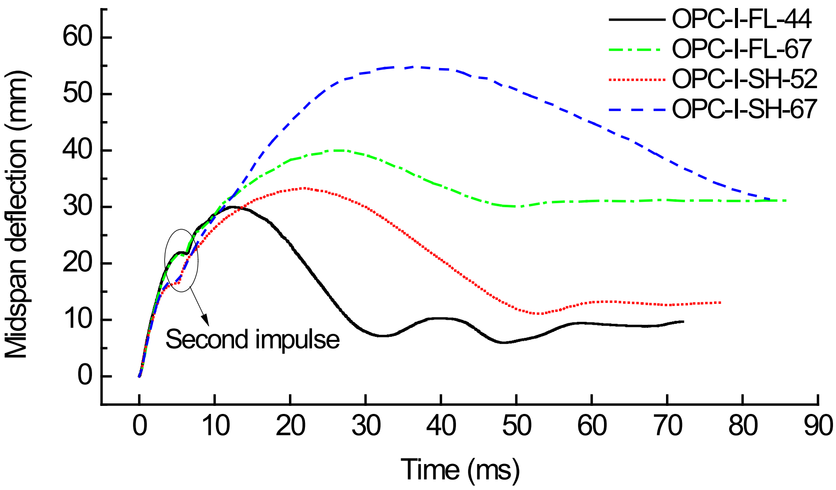

Fig. 10. Midspan deflection time histories of the beams

Fig. 11 presents the progressive failure of the tested beams. For Beam OPC-I-FL-44, two flexural cracks and a very short longitudinal crack at the bottom appeared at the instance of 1 ms. At 2 ms, another flexural crack near the existing left one and two new flexure-shear cracks close to the supports were observed. These cracks then further extended and became wider and nearly no new crack appeared after 7 ms. For Beam OPC-I-FL-67, two flexural cracks were observed at 1 ms. Some flexure-shear, shear, and longitudinal cracks developed on the beam from 2 ms to 3 ms. At 5 ms, very wide longitudinal cracks were noticed, which led to subsequent concrete spalling at the bottom. As can be seen at 7 ms, the cracks extended to the compression zone beneath the load cell adaptor and the concrete subsequently started crushing for both Beams OPC-I-FL-44 and OPC-I-FL-67 due to the global bending deflection of the beams, which was about 24 mm as shown in **Fig. 10**. For Beam OPC-I-SH-52, a shear crack, two flexural cracks, and some short longitudinal cracks were observed at 1 ms. More flexure-shear cracks appeared on the beam at 2 ms and there was no obvious change of the main crack pattern of the beam after 3 ms. The existing cracks then gradually extended and became wider, accompanied with the development of some short and secondary cracks. Similarly, the main crack pattern of Beam OPC-I-SH-67 was formed at 3 ms, characterized by two wide diagonal cracks. After that, the main crack pattern of the beam had no significant change except that the existing cracks further extended and became wider.

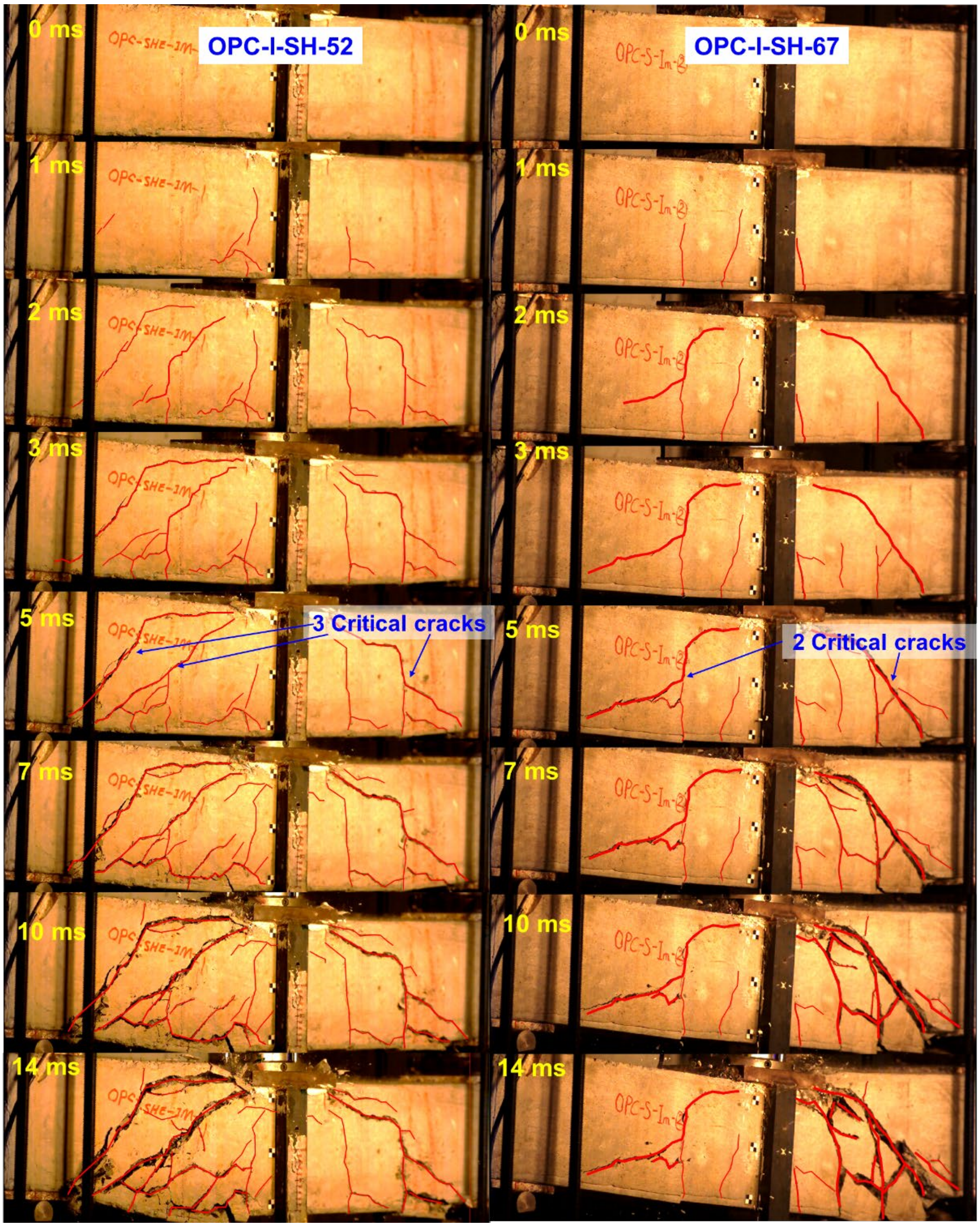

Fig. 11. Failure progress of the tested beams under impact loads

4.2. Dynamic responses

Each beam was only impacted once by the drop hammer with the dropping height of 2 m. **Table 3** gives the typical impact responses of the tested beams. It should be noted that the test data of the impact force and reinforcement strain of Beam OPC-I-FL-67 was lost due to malfunction of the data acquisition system. **Fig. 12** shows the time histories of the impact forces of the other three beams. As shown, the impact forces had the profile of two impulses. Beams OPC-I-FL-44 experienced the first impulse with the peak value of 418.0 kN and the duration of about 6 ms, followed by a second impulse with the peak value of 243.6 kN and the duration of about 3 ms. The impact force then exhibited a plateau with the value of about 75 kN from 9 ms to 16 ms and gradually decreased to 0 at 25 ms. The profiles of impact force were summarized and the factors that influence the profile of impact force were revealed in [52]. As compared to flexure-critical Beam OPC-I-FL-44, Beams OPC-I-SH-52 and OPC-I-SH-67 experienced lower first peak impulse with the values of 385.4 kN and 382.1 kN respectively, as well as shorter duration of about 5 ms. The two beams then experienced the second impulse with the peak values of 214.2 kN and 150.1 kN respectively, and the duration of about 5 ms. It was found that the second peak impulse of Beam OPC-I-SH-67 was smaller than that of Beam OPC-I-SH-52, which was caused by the reduced stiffness of Beam OPC-I-SH-67 after the first impulse as explained below. It should be noted that the actual impact velocities varied from 5.65 to 6.10 m/s, which could be due to different friction between the drop hammer and the guide tube from the different tests.

Table 3 Impact test results

Beam	Impact velocity (m/s)	Maximum impact force (kN)	Maximum deflection (mm)	Residual deflection (mm)	Residual capacity (kN)
OPC-I-FL-44	5.86	418.0	30.0	8.9	84.1
OPC-I-FL-67	6.10	*	40.0	31.1	-
OPC-I-SH-52	5.65	385.4	33.3	13.2	-
OPC-I-SH-67	5.77	382.1	54.8	31.4	-

Note: '*': data lost due to malfunction of the data acquisition system; '-': not tested due to severe damage of the beams after the impact tests.

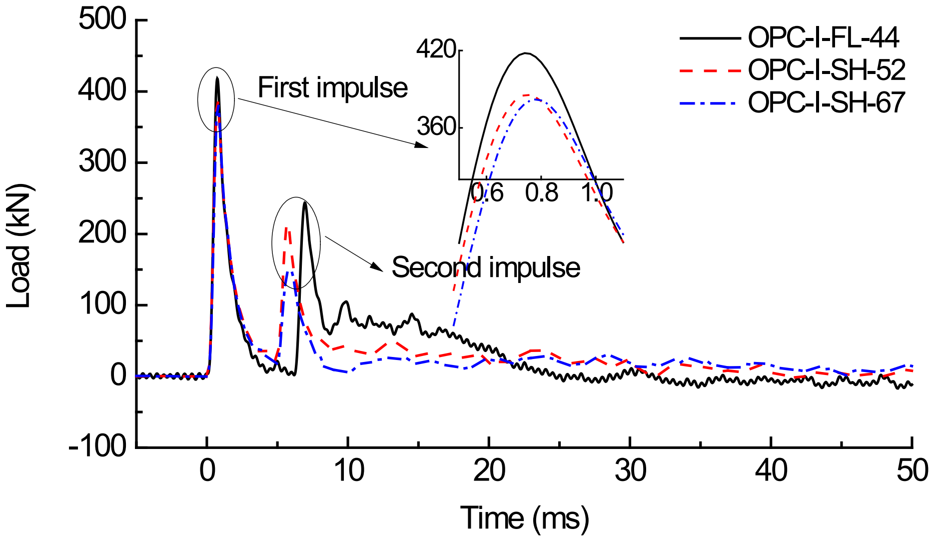

Fig. 12. Time histories of the impact forces of the tested beams

The midspan deflection time histories of the tested beams are shown in **Fig. 10**. The maximum deflection of Beams OPC-I-FL-44 and OPC-I-FL-67 was 30.0 mm and 40.0 mm, respectively, and their corresponding residual deflection was 8.9 mm and 31.1 mm, respectively. The maximum deflection of Beams OPC-I-SH-52 and OPC-I-SH-67 was 33.3 mm and 54.8 mm, respectively, and their corresponding residual deflection was 13.2 mm and 31.4 mm, respectively. Interestingly, both Beams OPC-I-FL-67 and OPC-I-SH-67 with higher concrete strength experienced larger maximum and residual deflection than Beams OPC-I-FL-44 and OPC-I-SH-52 with lower concrete strength. Other studies also observed this phenomenon, which was attributed to the increased brittleness of higher strength concrete [49-51]. In addition, it was reported that high strength concrete under dynamic loads was more sensitive to notch and required less fracture energy as compared to normal strength concrete [53]. Therefore, Beams OPC-I-FL-44 and OPC-I-SH-52 with lower concrete strength experienced more but narrower critical cracks whilst Beams OPC-I-FL-67 and OPC-I-SH-67 with higher concrete strength had less but wider critical cracks after the first impulse as shown in **Fig. 11** (at 5 ms). It should be noted that the shear resistance of beams was provided by dowel action of tension reinforcements, stirrups, aggregates interlocking, and shear resistance of concrete in compression zone [54]. As cracks widened, the shear resistance resisted by aggregates interlocking and dowel action reduced. Meanwhile, the contribution of concrete to the shear resistance of the beam in compression zone increased as reported in [54]. Since Beam OPC-I-SH-67 experienced similar impact force as Beam OPC-I-SH-52 (385.4 kN vs 382.1 kN) but wider critical cracks than Beam OPC-I-SH-52 as shown in **Fig. 11** (at 5 ms), it could be concluded that shear stress level at compression BFRP bars in Beam OPC-I-SH-67 was higher than that in Beam OPC-I-SH-52. It is noted that BFRP bars are prone to split under high shear stress [55], which might cause Beam OPC-I-SH-67 experiencing severer splitting damage of compression BFRP bars than Beam OPC-I-SH-52. The splitting damage of the compression BFRP bars could further decrease the stiffness of the beam, leading to a lower second peak impulse of Beam OPC-I-SH-67 (i.e., 150.1 kN) than that of Beam OPC-I-SH-52 (i.e., 214.2 kN) as shown in **Fig. 12** and higher damage level of the beam, as well as larger midspan deflection.

Fig. 13 displays the reinforcement strain time histories of the tested beams. Only TSG in Beam OPC-I-FL-44 completely captured the strain time history of the compression reinforcements, while LSG2 and SSG1 in Beam OPC-I-SH-52 and LSG1 in Beam OPC-I-SH-67 partially captured strain time histories of tension reinforcements and stirrups due to the rupture of strain gauge cables induced by cracks. Unfortunately, other strain gauges could not capture valid data either due to rupture of strain gauge cables or out of measurement range. The strain of the top longitudinal BFRP bars (TSG) of Beam OPC-I-FL-44 at midspan was negative (compressive) at the very beginning (from 0 to 0.4 ms) as shown in **Fig. 13**(a) enlarged due to the stress wave propagation, which was also observed in the simulation in Section 5.3. It then became positive (tensile) from 0.4 ms to 8 ms, which was attributed to change of the location of neutral axis above the compression BFRP bars as shown in **Fig. 13**(b) (see 4 ms). This phenomenon was also verified by the simulation in Section 5.3. After 7 ms, the concrete cover began crushing as shown in **Fig. 11** (at 7 ms) and the concrete cover could not resist compressive stress, thereby the compression zone and neutral axis moved downwards as shown in **Fig. 13**(b) (see 15 ms). This phenomenon was also observed and explained in the previous study [56]. Therefore, the strain of TSG changed to negative (compressive) from about 8 ms to 24 ms. Finally, it rebounded back to positive (tensile) and fluctuated during the free vibration phase and ended with a small positive (tensile) residual strain of about 1000 $\mu\varepsilon$, which might be resulted from the compression zone moving downwards further as shown in **Fig. 13**(b) (see 70 ms) due to the crushed areas at the midspan, corresponding to the severe concrete crushing damage as shown in **Fig. 9** and **Fig. 11**. The strain of tension reinforcements (LSG2) of Beam OPC-I-SH-52 increased faster than that of stirrups (SSG1) as shown in **Fig. 13**(a) since the flexural cracks appeared earlier than shear cracks. Both of them increased to the first peak at about 5 ms after the first impulse, e.g. around 9,000 με and 3,000 με, respectively. The strain of tension reinforcements (LSG2) subsequently reached the second peak of about 8,000 με with the development of cracks after the second impulse. The LSG1 in Beam OPC-I-SH-67 only captured the first peak of about 6,000 με and then failed due to the rupture of strain gauge cable.

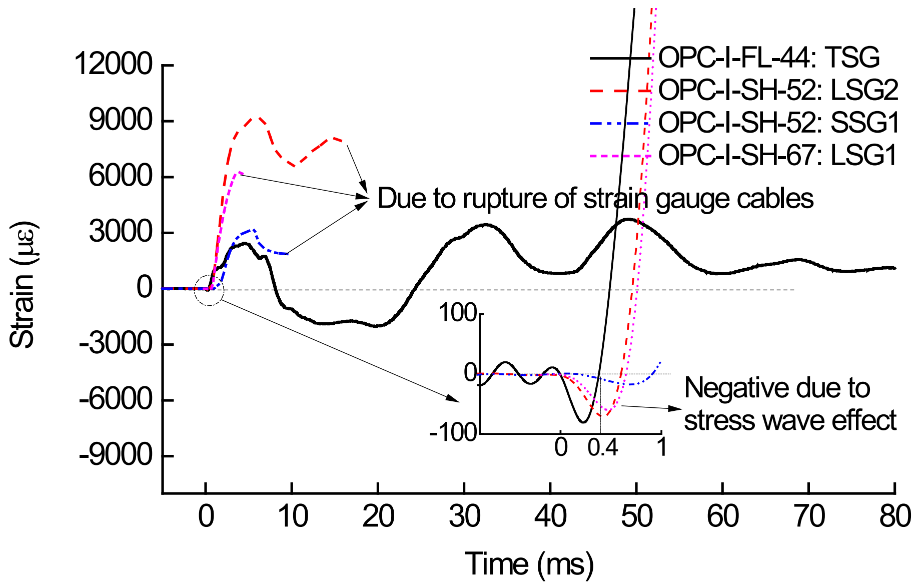

(a)

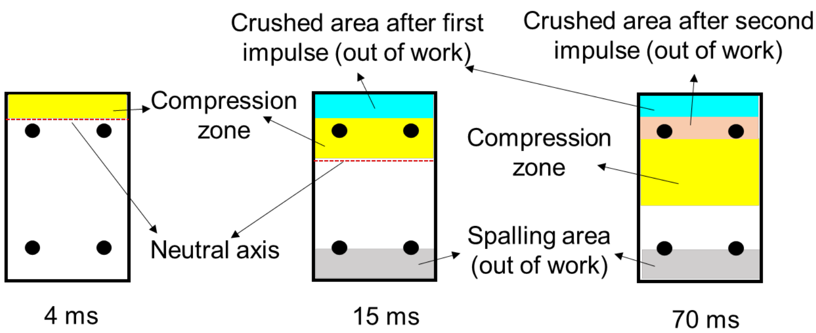

(b)

Fig. 13. (a) Strain time histories of reinforcements in Beam OPC-I-FL-44, and (b) schematic diagram of neutral axis at midspan section at various instants

4.3. Residual load-carrying capacity of the tested beams

The residual load-carrying capacity of concrete beams after the impact tests could be used to evaluate the damage level of concrete beams based on some indices [36, 57] such as the ratio of the post-impact residual load-carrying capacity to the load-carrying capacity of the beams without impact testing. Since Beams OPC-I-FL-67, OPC-I-SH-52, and OPC-I-SH-67 experienced very severe damage with relatively large residual deflection under impact loads, only Beam OPC-I-FL-44 was further tested under monotonic quasi-static loads to obtain the residual load-carrying capacity. **Fig. 14** shows the failure mode of Beam OPC-I-FL-44 before and after the residual load-carrying capacity test. It can be seen that more concrete crushing on the top and concrete spalling at the bottom were observed as indicated in the figure. **Fig. 15** displays the load-midspan deflection curve from the residual load-carrying capacity test. The beam had a residual load-carrying capacity of 84.1 kN and experienced a brittle failure with the applied load decreased suddenly after the applied load reached the residual load-carrying capacity.

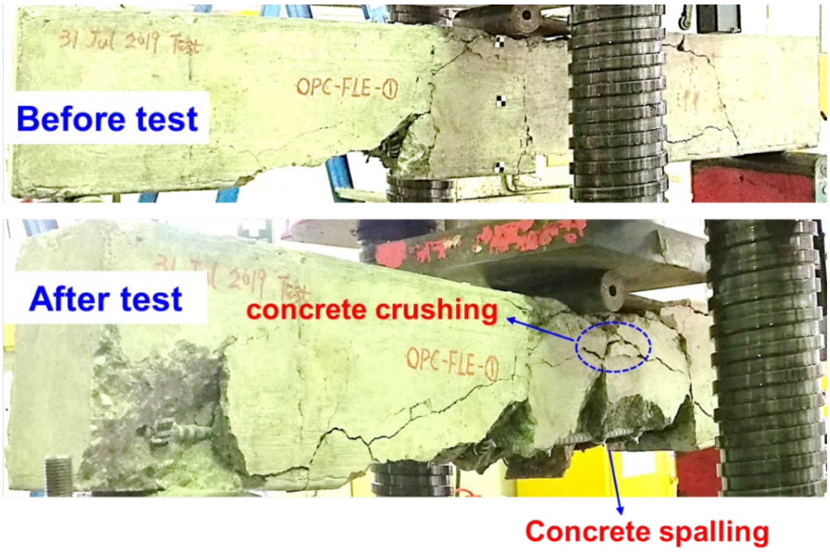

Fig. 14. Residual capacity test of Beam OPC-I-44

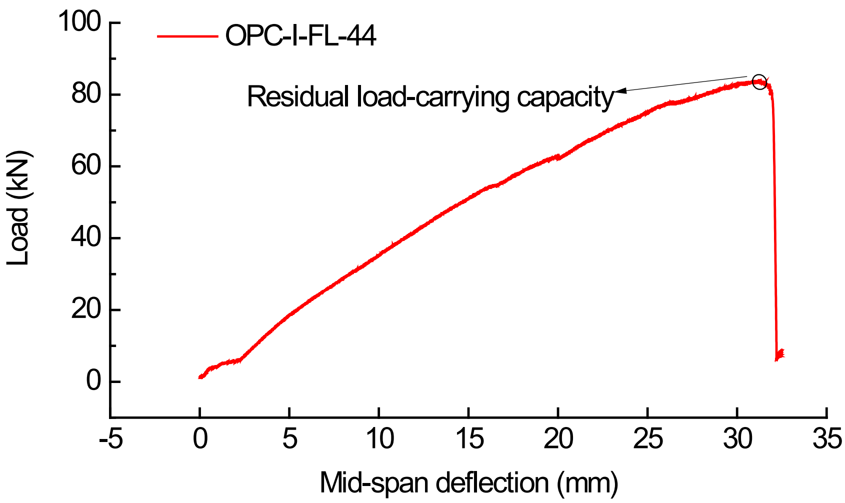

Fig. 15. Load-midspan deflection curve of Beam OPC-I-FL-44 from post-impact residual load-carrying capacity test

5. Numerical simulations

5.1. Finite element model

In this section, the numerical simulations were conducted by using commercial software LS-DYNA [58], which have been widely used to simulate RC structures subjected to impact and blast loads and proven yielding reliable numerical predictions [24, 59]. The test results of Beam OPC-I-FL-44 were utilized for the calibration against the numerical results since this beam had more complete data than other three beams. The developed numerical model is shown in **Fig. 16**. Eight-node solid elements were utilized for all parts except the BFRP reinforcements. The longitudinal BFRP reinforcements and stirrups were modelled using Hughes-Liu beam elements with cross section integration. The supports were simplified without considering threaded rods between the steel plates so that the boundaries were simulated by constraining the outer plates and the steel rollers in all directions. After conducting mesh sensitivity analysis, a mesh size of 7.5 mm was selected for concrete beams and reinforcements while a mesh size of 10 mm was determined for other parts to balance the accuracy and efficiency. The interaction between the reinforcements and concrete was simulated using the keyword *Constrained_Beam_in_Solid. The keyword *Automatic_Surface_to_Surface contact was adopted to model the contacts among the drop hammer, load cell cap, load cell, and load cell adaptor, concrete, steel plates, and steel rollers, while the keyword *Automatic_Surface_to_Surface_Tiebreak contact was employed to simulate the connection between the load cell and the load cell adaptor. The keyword *Initial_Velocity_Generation was used to specify an initial impact velocity for the drop hammer, which was 5.86 m/s based on the test results as listed in **Table 3**.

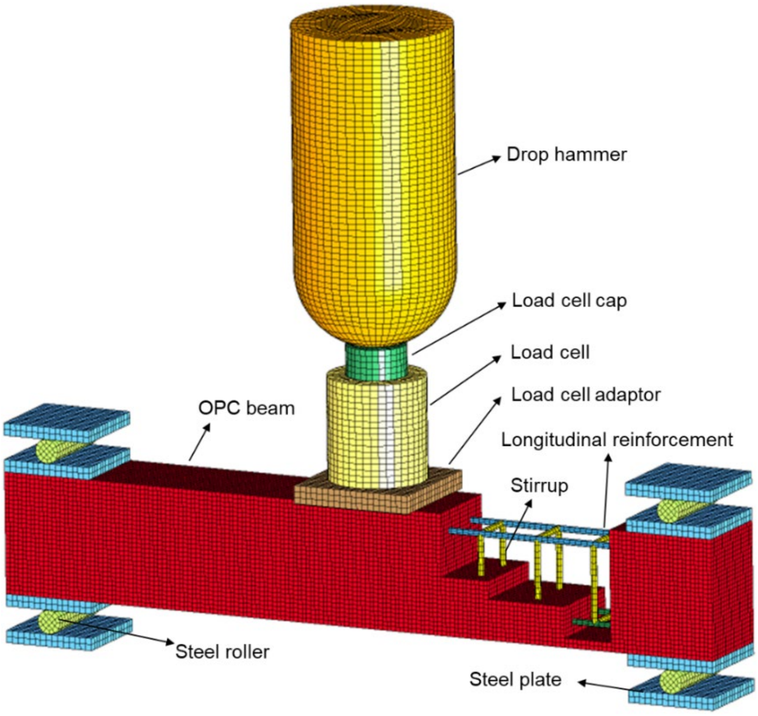

Fig. 16 Numerical model

5.2. Material models

In this study, *Mat_Concrete_Damage_Rel3 (*Mat_072R3, also called KCC model) was used for modelling concrete, while *Mat_Piecewise_Linear_Plasticity (*Mat_024) was employed to model other parts. The parameters of material models are listed in **Table 4**. Considering the configuration of internal gap inside the load cell, the load cell was simplified as a solid mass and its density was determined by the equivalent mass density, i.e., the ratio of the actual mass to the external volume of the modelled load cell, which was 5850 kg/m^3, about 25% lower than the density of steel material. For simplicity and without changing the propagating velocity of stress wave inside the load cell, the equivalent modulus of the modelled load cell was also taken as 150 GPa, 25% lower than the actual modulus of steel material.

Table 4 Parameters of material model

Parts	Material model in LS-DYNA	Parameter	Value
concrete	Concrete_Damage_Rel3 (*Mat_072R3)	Density	2300 kg/m^3
		Poisson's ratio	0.2

		Compressive strength	44 MPa
BFRP reinforcements	Piecewise_Linear_Plasticity (*Mat_024)	Density	2000 kg/m^3
		Modulus of elasticity	55 GPa
		Poisson's ratio	0.25
		Tensile strength	1200 MPa
		Effective plastic failure strain	1.0E-5
Load cell	Piecewise_Linear_Plasticity (*Mat_024)	Density	5850 kg/m^3
		Modulus of elasticity	150 GPa
		Poisson's ratio	0.3
		Yield stress	500 MPa
Steel plates, steel rollers, drop hammer, load cell cap, load cell adaptor	Piecewise_Linear_Plasticity (*Mat_024)	Density	7800 kg/m^3
		Modulus of elasticity	200 GPa
		Poisson's ratio	0.3
		Yield stress	500 MPa

The strain rate effect was considered in the present study. Both material models *Mat_72R3 and *Mat_024 allow users to define strength increment with a dynamic increase factor (DIF) at a given strain rate. The DIFs of concrete, BFRP composites, and steel material could refer to [60], [61], and [62], respectively. To model the physical fracture of material and avoid computation overflow due to large distortion of elements, the erosion algorithm was utilized by given erosion criteria via the keyword *Mat_Add_Erosion, which has been widely used in concrete structures subjected to impact and blast loads [24, 25]. In this simulation, the erosion criteria including maximum principal strain of 0.14 for concrete, minimum principal strain of -0.011 ('-' denotes tension) for the stirrups, shear strain of 0.09 for the top longitudinal BFRP bars, and effective plastic failure strain of 1.0E-5 (see **Table 4**) for the bottom longitudinal BFRP bars, were determined by trial-and-error to achieve good agreement between the numerical and test results.

5.3. Comparison between the numerical and test results

Fig. 17 and **Fig. 18** show the comparisons between the numerical and test results in terms of failure progress and impact responses of Beam OPC-I-FL-44, respectively. The numerical results are in good agreement with the test results in general. As shown in **Fig. 17**, the effective plastic strain contour from the numerical simulation can reflect the crack patterns of the tested beam including concrete spalling at the bottom and concrete crushing on the top. The comparisons of impact force, midspan deflection, and the strain of TSG are shown in **Fig. 18**. The impact force in the numerical simulation was retrieved by the contact force of the interface between the load cell cap and the load cell. The peak impact forces from the numerical and test results were 413.3 kN and 418.0 kN, respectively. The maximum and residual displacements from the numerical simulation were 29.6 mm and 5.0 mm, respectively, and the corresponding values from the test results were 30.0 mm and 8.9 mm, respectively. It should be noted that the numerical simulation could well capture the trend (i.e. tension and compression) of strain time history of TSG. However, the numerical simulation over predicted TSG strain although similar displacement was predicted, which might be due to the element erosion. In the testing, the concrete near the top longitudinal BFRP bars experienced severe crushing damage but could still sustain compressive load. However, in the numerical simulation, once reaching the defined erosion criteria the concrete elements near the top longitudinal reinforcements were eroded and could not resist load, resulting in a higher strain in top reinforcements as compared to the testing results. Overall, the time histories of impact force, midspan deflection, and the trend of strain time history of TSG were reasonably predicted by the numerical simulation.

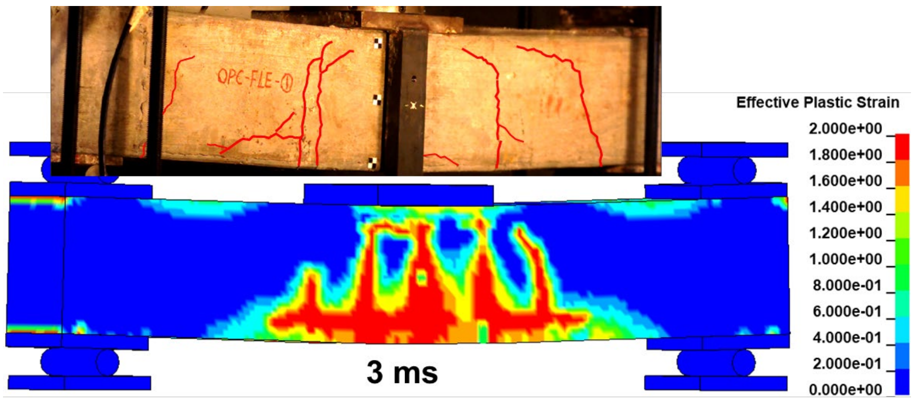

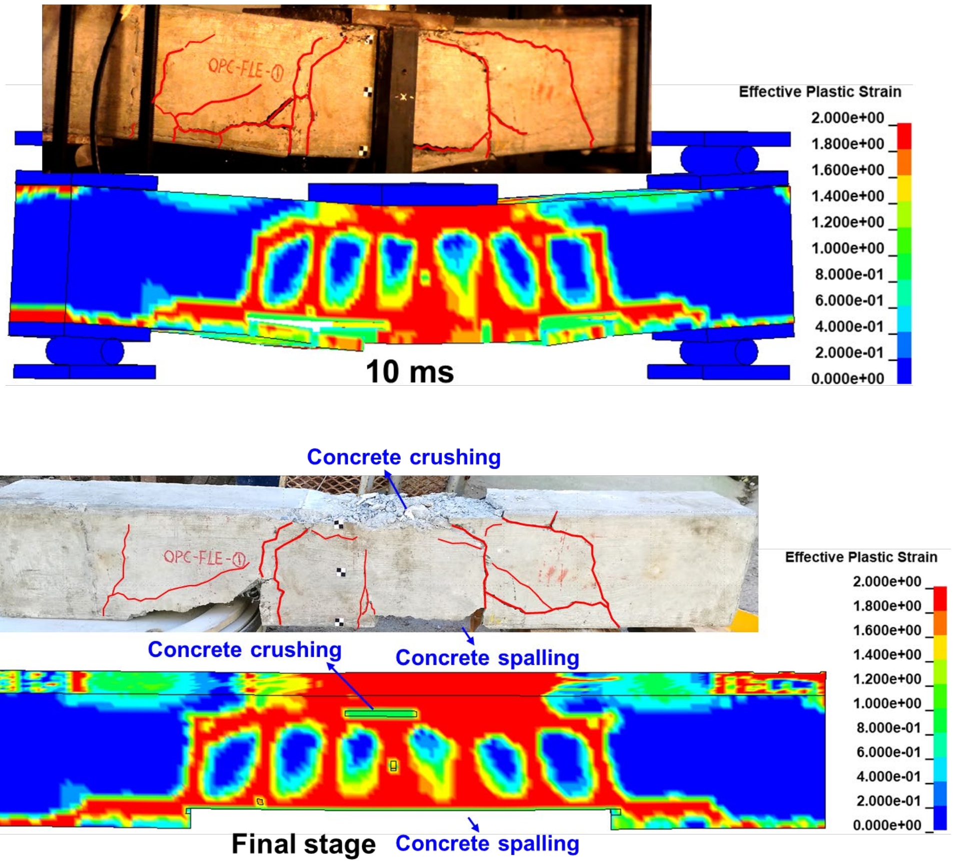

Fig. 17 Comparison of crack pattern and failure mode of Beam OPC-I-FL-44

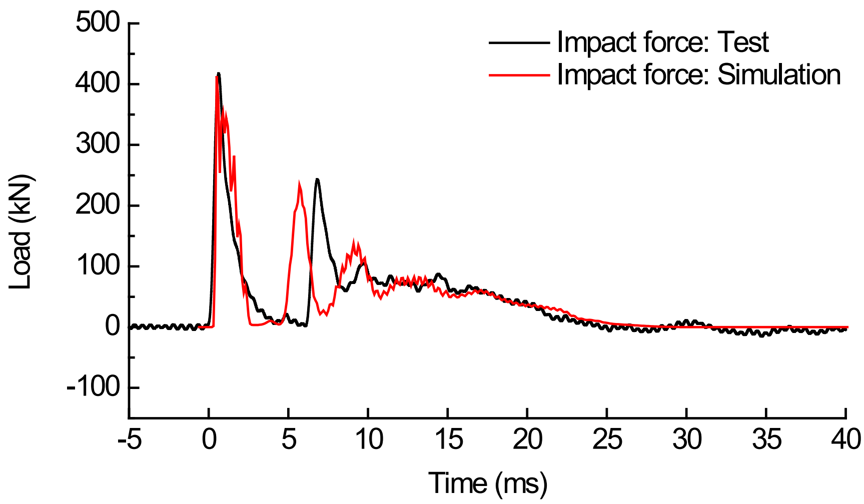

(a)

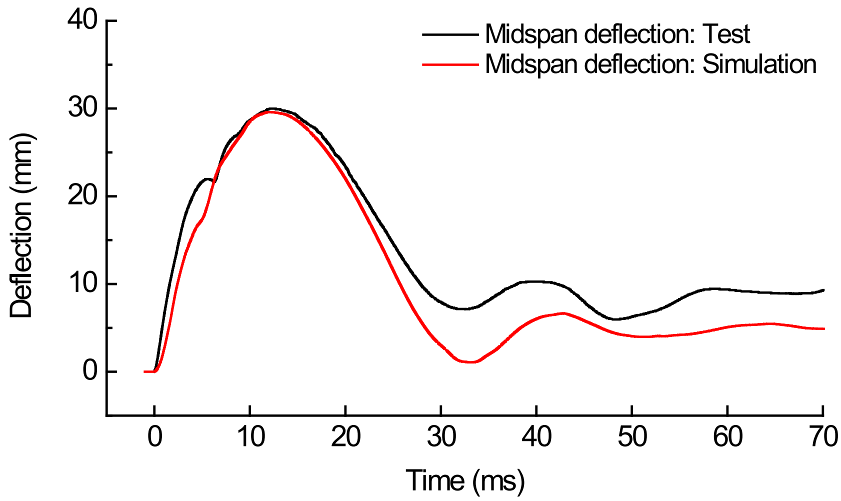

(b)

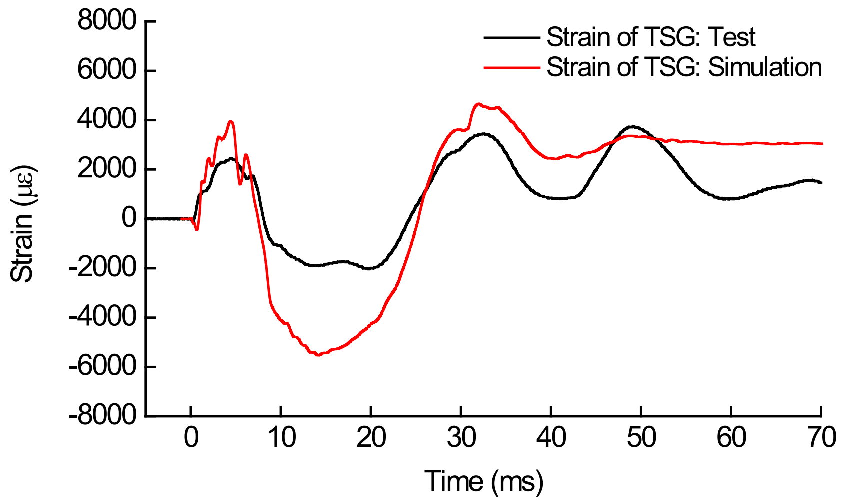

(c)

Fig. 18 Comparison of impact responses: (a) impact force, (b) midspan deflection, and (c) strain of TSG

6. Parametric study

6.1. Effect of tension reinforcement ratio

Tension reinforcement ratio greatly affects the load-carrying capacity and deformational response of concrete beams. Therefore, based on the validated numerical model, further studies were performed to investigate the influence of the tension reinforcement ratio on the impact performance of concrete beams reinforced with BFRP bars. In this section, four reinforcement ratios of 0.41%, 0.63%, 0.91%, and 1.24% were considered by varying the diameters of the tension BFRP bars, which were 8 mm, 10 mm, 12 mm, and 14 mm, respectively. **Fig. 19** and **Fig. 20** show the failure modes and midspan deflection time histories of the beams with varying reinforcement ratios, respectively. Only the beam with reinforcement ratio of 0.41% experienced rupture damage of tension BFRP bars, thus leading to a larger maximum and residual midspan deflection of the beam as compared to the beams with higher reinforcement ratios. With the increased reinforcement ratio (i.e. the designed shear-flexural capacity ratio of the beams decreased from 2.3 to 1.6), the damage of the beam was more concentrated on the impact area and the failure modes of the beams shifted from flexure-governed to flexure-shear combined. The maximum midspan deflection of the beams reduced with the increased reinforcement ratio.

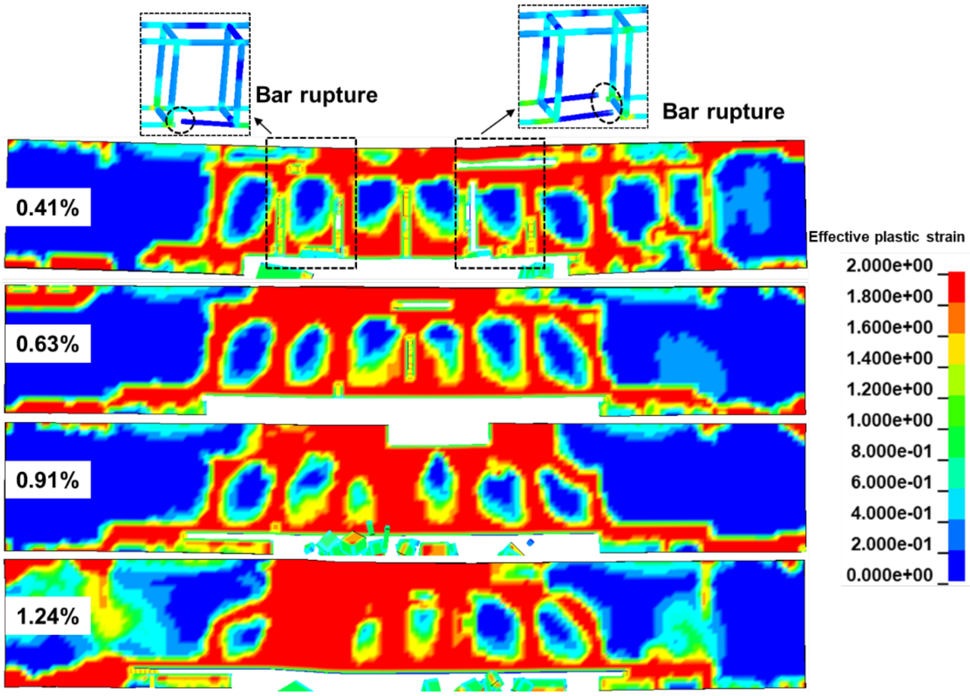

Fig. 19 Failure modes of the beams with varying tension reinforcement ratios under impact loads

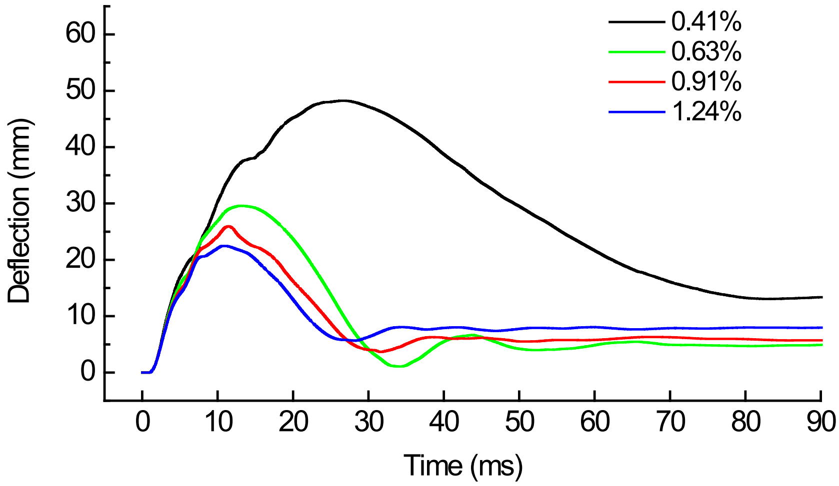

Fig. 20. Midspan deflection time histories of the beams with varying tension reinforcement ratios under impact loads

6.2. Effect of reinforcement type

To investigate the effect of reinforcement material on the impact performance of concrete beams, a conventional RC beam (B-Steel) and a concrete beam reinforced with BFRP bars (B-BFRP) are compared. The conventional RC beam (B-Steel) was simulated by replacing BFRP material with steel material for longitudinal and transverse reinforcements in the calibrated numerical model. The material model and parameters for steel plates as listed in **Table 4** were employed for steel reinforcements. **Fig. 21** shows the comparison of failure modes between Beams B-BFRP and B-Steel. As can be seen, Beam B-BFRP experienced flexure-shear combined damage while Beam B-Steel exhibited flexural damage. Wider flexural cracks (illustrated by deleted elements) at the midspan of Beam B-Steel were observed as compared to those on Beam B-BFRP. **Fig. 22** shows the comparisons of the dynamic responses between Beams B-BFRP and B-Steel with respect to the midspan deflection, axial stress and axial strain of tension reinforcements at midspan. As compared to Beam B-BFRP, Beam B-Steel experienced slightly larger maximum midspan deflection (31.1 mm vs 29.6 mm) and much larger residual midspan deflection (27.8 mm vs 5.0 mm) as shown in **Fig. 22**(a). The maximum tensile stress (i.e. 1096 MPa) in the tension BFRP bars of Beam B-BFRP as shown in **Fig. 22**(b) did not even reach the static tensile strength of BFRP bars (i.e. 1200 MPa). Due to the nature of BFRP rebar which is a linear elastic material, it could recover to its original state, leading to a very small residual deflection of the beam, e.g. 5.0 mm as shown in **Fig. 22**(a). However, the tensile stress in tension steel bars of Beam B-Steel reached a relatively constant value of about 660 MPa (induced by strain rate effect with a DIF 1.3, i.e., 660 MPa /500 MPa) from 1 ms to 15 ms as shown in **Fig. 22**(b), while their strain increased from 4.1E3 με to 1.6E5 με in the same time period (i.e. 1-15 ms) as shown in **Fig. 22**(c). This meant the tension steel bars in Beam B-Steel yielded, thereby Beam B-Steel experienced much larger residual midspan deflection (i.e. 27.8 mm) than that of Beam B-BFRP (i.e. 5.0 mm). From these observations, it could be concluded that the impact performance of flexure-critical concrete beams reinforced with BFRP bars is comparable to that of conventional RC beams with steel bars. It should be mentioned that this conclusion may not be applicable for flexure-critical concrete beams with tension reinforcement ratio less than 0.41% since the beams reinforced with BFRP bars could experience rupture damage of tension BFRP bars owing to their less deformation capability as compared to steel bars and thus may lead to an adverse effect as demonstrated in section 6.1.

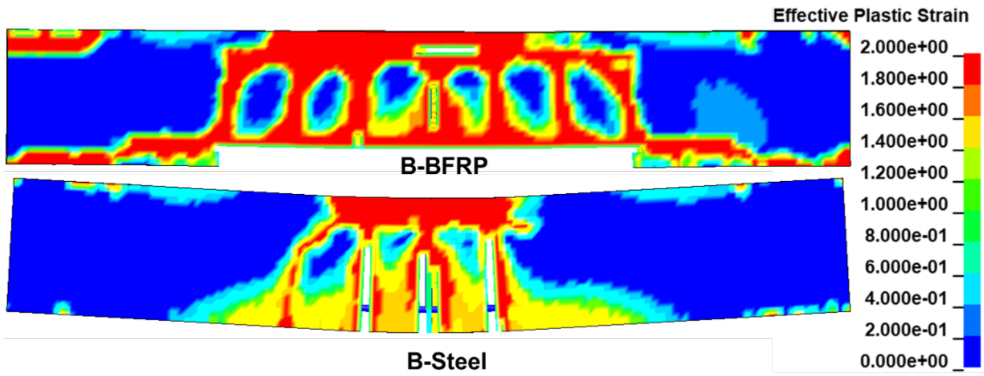

Fig. 21 Comparison of failure modes between conventional RC beams and concrete beams reinforced with BFRP bars

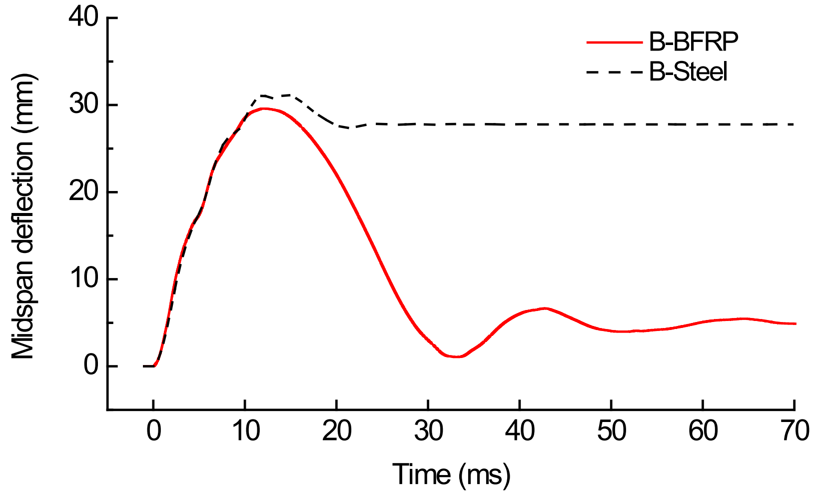
B-BFRP
B-Steel
Midspan deflection (mm)
Time (ms)
0
10
20
30
40
50
60
70

(a)

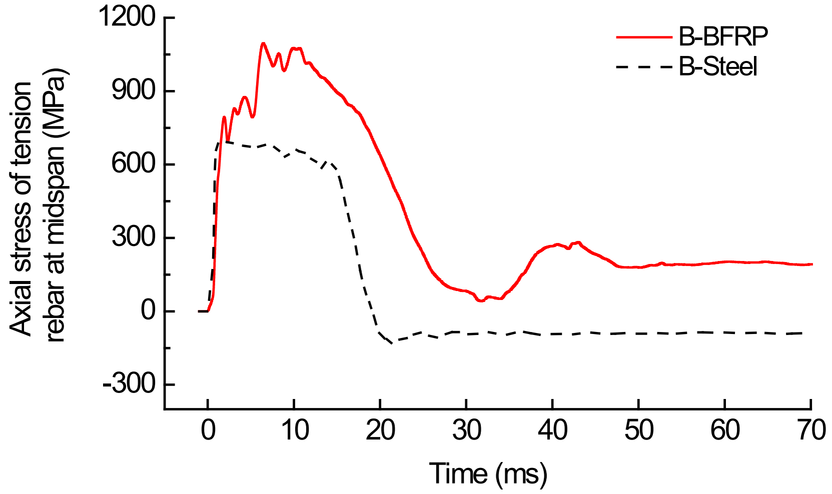
B-BFRP
B-Steel
Axial stress of tension rebar at midspan (MPa)
Time (ms)
-300
0
300
600
900
1200

(b)

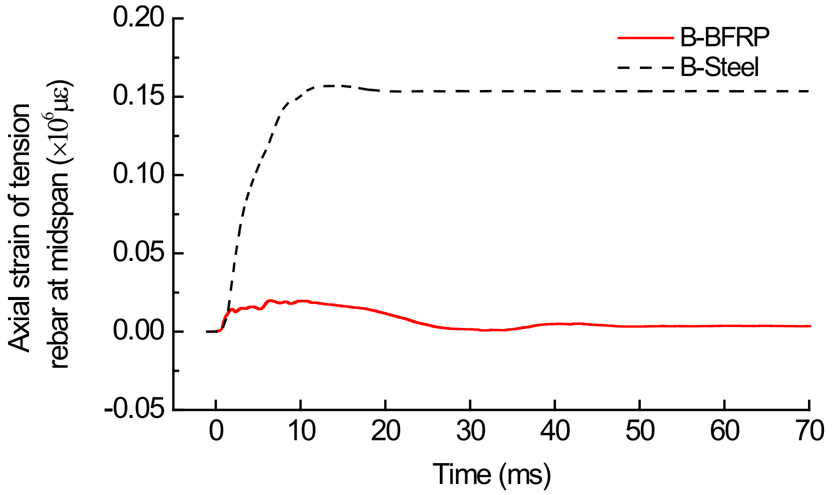
B-BFRP
B-Steel
Axial strain of tension rebar at midspan (×10^{6}με)
Time (ms)
-0.05
0.00
0.05
0.10
0.15
0.20

(c)

Fig. 22. Comparison of dynamic responses between conventional RC beams and concrete beams reinforced with BFRP bars: (a) midspan deflection, (b) axial stress of tension rebars, and (c) axial strain of tension rebars at midspan

7. Conclusion

In this study, quasi-static and impact tests were conducted on flexure-critical and shear-critical concrete beams reinforced with BFRP bars. Two beams as reference beams were tested under quasi-static loads and four beams were tested under impact loads. The test results were examined and discussed. Numerical model was also developed and calibrated against the impact test results. The calibrated numerical model was then used to further investigate the effect of tension reinforcement ratio and reinforcements material on the impact performance of the beams. Based on the test and numerical results, the conclusions can be drawn as follows:

1. The flexure-critical beam and the shear-critical beam under quasi-static loads failed in flexure and shear, respectively, as expected. The load-midspan deflection curves of these two beams were generally bilinear up to the peak load. ACI 440.1R-15 [14] underestimates the static flexural capacity and the static shear capacity of the tested beams by 26% and 53%, respectively.

2. The flexure-critical concrete beam reinforced with BFRP bars experienced the failure mode changing from flexure-governed under quasi-static loads to flexure-shear combined under impact loads. The shear-critical concrete beams reinforced with BFPR bars under impact loads still failed in diagonal shear, but experienced severer concrete spalling and more critical diagonal cracks on both sides of the beams as well as wider distribution area of cracks than those subjected to quasi-static loads.

3. Increasing the concrete strength but reducing its deformation capability degrade the impact resistance performance of concrete beams reinforced with BFRP bars, resulting in larger maximum and residual midspan deflection of the beams, and even severer splitting damage to the top longitudinal BFRP bars for shear-critical beams due to the increased brittleness of concrete.

4. The numerical results of the beam under impact loads agreed well with the test results. Numerical results showed that increasing the tension reinforcement ratio (i.e. decreasing shear-flexural capacity

ratio) could change the failure mode of the flexure-critical beams from flexure-governed to flexure-shear combined with reduced maximum midspan deflection.

5. In general, the structural performance of flexure-critical concrete beams reinforced with BFRP bars under impact loads was comparable to that of conventional RC beams with steel bars in this study. Therefore, BFRP bars could be used as an alternative to reinforce concrete beams.

8. Acknowledgements

This work was supported by the Australian Research Council (ARC) via Australian Laureate Fellowship (FL180100196).

9. References

[1] T.A. El Maaddawy, K.A. Soudki, Effectiveness of impressed current technique to simulate corrosion of steel reinforcement in concrete, J. Mater. Civ. Eng. 15(1) (2003) 41-47.

[2] H.V. GangaRao, N. Taly, P. Vijay, Reinforced concrete design with FRP composites, CRC press, Boca Raton, Florida, 2006.

[3] I.F. Kara, A.F. Ashour, Flexural performance of FRP reinforced concrete beams, Compos. Struct. 94(5) (2012) 1616-1625.

[4] C.H. Kim, H.S. Jang, Concrete shear strength of normal and lightweight concrete beams reinforced with FRP bars, J. Compos. Constr. 18(2) (2013) 04013038.

[5] E. Oller, A. Marí, J.M. Bairán, A. Cladera, Shear design of reinforced concrete beams with FRP longitudinal and transverse reinforcement, Compos Part B-Eng 74 (2015) 104-122.

[6] F. Elgabbas, P. Vincent, E.A. Ahmed, B. Benmokrane, Experimental testing of basalt-fiber-reinforced polymer bars in concrete beams, Compos Part B-Eng 91 (2016) 205-218.

[7] W.-r. Yang, X.-j. He, L. Dai, Damage behaviour of concrete beams reinforced with GFRP bars, Compos. Struct. 161 (2017) 173-186.

[8] J. Duic, S. Kenno, S. Das, Performance of concrete beams reinforced with basalt fibre composite rebar, Constr. Build. Mater. 176 (2018) 470-481.

[9] O.I. Abdelkarim, E.A. Ahmed, H.M. Mohamed, B. Benmokrane, Flexural strength and serviceability evaluation of concrete beams reinforced with deformed GFRP bars, Eng. Struct. 186 (2019) 282-296.

[10] Y. Yuan, Z. Wang, Shear behavior of large-scale concrete beams reinforced with CFRP bars and handmade strip stirrups, Compos. Struct. 227 (2019) 111253.

[11] S. Cholostiakow, M. Di Benedetti, K. Pilakoutas, E. Zappa, M. Guadagnini, Experimental Analysis of Shear Resisting Mechanisms in FRP RC Beams with Shear Reinforcement, J. Compos. Constr. 24(5) (2020) 04020037.

[12] S. Kueres, N. Will, J. Hegger, Shear strength of prestressed FRP reinforced concrete beams with shear reinforcement, Eng. Struct. 206 (2020).

[13] CSA S806-12, Design and construction of building structures with fibre-reinforced polymers, Canadian Standards Association, Ontario, Canada, 2012.

[14] ACI 440.1R-15, Guide for the design and construction of concrete reinforced with Fiber Rienforced Polymers (FRP) bars, American Concrete Institute, Farmington Hills, MI, USA, 2015.

[15] N. Kishi, O. Nakano, K. Matsuoka, T. Ando, Experimental study on ultimate strength of flexural-failure-type RC beams under impact loading, (2001).

[16] N. Kishi, H. Mikami, K. Matsuoka, T. Ando, Impact behavior of shear-failure-type RC beams without shear rebar, Int. J. Impact Eng. 27(9) (2002) 955-968.

[17] K. Fujikake, B. Li, S. Soeun, Impact response of reinforced concrete beam and its analytical evaluation, J. Struct. Eng. 135(8) (2009) 938-950.

[18] S. Saatci, F.J. Vecchio, Effects of Shear Mechanisms on Impact Behavior of Reinforced Concrete Beams, ACI Struct. J. 106(1) (2009) 78-86.

[19] S.D. Adhikary, B. Li, K. Fujikake, Strength and behavior in shear of reinforced concrete deep beams under dynamic loading conditions, Nucl. Eng. Des. 259 (2013) 14-28.

[20] S.D. Adhikary, B. Li, K. Fujikake, Low velocity impact response of reinforced concrete beams: experimental and numerical investigation, International Journal of Protective Structures 6(1) (2015) 81-111.

[21] D.-B. Zhao, W.-J. Yi, S.K. Kunnath, Shear mechanisms in reinforced concrete beams under impact loading, J. Struct. Eng. 143(9) (2017) 04017089.

[22] Q. Yan, B. Sun, X. Liu, J. Wu, The effect of assembling location on the performance of precast concrete beam under impact load, Adv. Struct. Eng. 21(8) (2018) 1211-1222.

[23] T.M. Pham, H. Hao, Impact Behavior of FRP-Strengthened RC Beams without Stirrups, J. Compos. Constr. 20(4) (2016).

[24] D.-B. Zhao, W.-J. Yi, S.K. Kunnath, Numerical simulation and shear resistance of reinforced concrete beams under impact, Eng. Struct. 166 (2018) 387-401.

[25] H. Li, W. Chen, H. Hao, Influence of drop weight geometry and interlayer on impact behavior of RC beams, Int. J. Impact Eng. 131 (2019) 222-237.

[26] Y. Fu, X. Yu, X. Dong, F. Zhou, J. Ning, P. Li, Y. Zheng, Investigating the failure behaviors of RC beams without stirrups under impact loading, Int. J. Impact Eng. 137 (2020).

[27] Y. Chen, I.M. May, Reinforced concrete members under drop-weight impacts, Proceedings of the Institution of Civil Engineers-Structures and Buildings, 2009, pp. 45-56.

[28] N. Kishi, H. Mikami, Empirical Formulas for Designing Reinforced Concrete Beams under Impact Loading, ACI Struct. J. 109(4) (2012).

[29] H. Ohnuma, C. Ito, S. Nomachi, Dynamic response and local rupture of reinforced concrete beam and slab under impact loading, (1985).

[30] W.-J. Yi, D.-B. Zhao, S.K. Kunnath, Simplified Approach for Assessing Shear Resistance of Reinforced Concrete Beams under Impact Loads, ACI Struct. J. 113(4) (2016).

[31] A.Q. Bhatti, N. Kishi, H. Mikami, T. Ando, Elasto-plastic impact response analysis of shear-failure-type RC beams with shear rebars, Mater. Des. 30(3) (2009) 502-510.

[32] A. Nanni, A.D. Luca, H.J. Zadeh, Reinforced Concrete with FRP Bars - Mechanics and Design, CRC Press, Boca Raton, Florida, USA, 2014.

[33] M. Goldston, A. Remennikov, M.N. Sheikh, Experimental investigation of the behaviour of concrete beams reinforced with GFRP bars under static and impact loading, Eng. Struct. 113 (2016) 220-232.

[34] M.W. Goldston, A. Remennikov, Z. Saleh, M.N. Sheikh, Experimental investigations on the behavior of GFRP bar reinforced HSC and UHSC beams under static and impact loading, Structures 22 (2019) 109-123.

[35] Z. Saleh, M.N. Sheikh, A. Remennikov, A. Basu, Numerical Analysis of Behavior of Glass Fiber-Reinforced Polymer Bar-Reinforced Concrete Beams under Impact Loads, ACI Struct. J. 116(5) (2019) 151-160.

[36] Z. Saleh, M.N. Sheikh, A. Remennikov, A. Basu, Overload Damage Mechanisms of GFRP-RC Beams Subjected to High-intensity Low-velocity Impact Loads, Compos. Struct. (2019) 111578.

[37] Z. Saleh, M.N. Sheikh, A. Remennikov, A. Basu, Damage assessment of GFRP bar reinforced ultra-high-strength concrete beams under overloading impact conditions, Eng. Struct. 213 (2020) 110581.

[38] Y.M. Amran, R. Alyousef, R.S. Rashid, H. Alabduljabbar, C.-C. Hung, Properties and applications of FRP in strengthening RC structures: A review, Structures, Elsevier, 2018.

[39] Z. Wang, X.-L. Zhao, G. Xian, G. Wu, R.S. Raman, S. Al-Saadi, A. Haque, Long-term durability of basalt-and glass-fibre reinforced polymer (BFRP/GFRP) bars in seawater and sea sand concrete environment, Constr. Build. Mater. 139 (2017) 467-489.

[40] Z. Huang, W. Chen, H. Hao, Z. Chen, T.M. Pham, T.T. Tran, M. Elchalakani, Flexural Behaviour of Ambient Cured Geopolymer Concrete Beams Reinforced with BFRP Bars under Static and Impact Loads, Compos. Struct. (accepted) (2020).

[41] Z. Huang, W. Chen, H. Hao, Z. Chen, T.M. Pham, T.T. Tran, M. Elchalakani, Shear Behaviour of Ambient Cured Geopolymer Concrete Beams Reinforced with BFRP Bars under Static and Impact Loads, (under review) (2020).

[42] R.J. Thomas, S. Peethamparan, Alkali-activated concrete: Engineering properties and stress–strain behavior, Constr. Build. Mater. 93 (2015) 49-56.

[43] N.A. Farhan, M.N. Sheikh, M.N. Hadi, Investigation of engineering properties of normal and high strength fly ash based geopolymer and alkali-activated slag concrete compared to ordinary Portland cement concrete, Constr. Build. Mater. 196 (2019) 26-42.

[44] Jiangsu Green Materials Vally New Material T&D Co. Ltd (GMV), Basalt Fiber Composite Bar.

[45] M.W. Goldston, A. Remennikov, M.N. Sheikh, Flexural behaviour of GFRP reinforced high strength and ultra high strength concrete beams, Constr. Build. Mater. 131 (2017) 606-617.

[46] G.B. Maranan, A.C. Manalo, B. Benmokrane, W. Karunasena, P. Mendis, Evaluation of the flexural strength and serviceability of geopolymer concrete beams reinforced with glass-fibre-reinforced polymer (GFRP) bars, Eng. Struct. 101 (2015) 529-541.

[47] A. El Refai, F. Abed, Concrete contribution to shear strength of beams reinforced with basalt fiber-reinforced bars, J. Compos. Constr. 20(4) (2015) 04015082.

[48] M.S. Alam, A. Hussein, Unified shear design equation for concrete members reinforced with fiber-reinforced polymer without stirrups, J. Compos. Constr. 17(5) (2012) 575-583.

[49] A.N. Dancygier, D.Z. Yankelevsky, Effects of reinforced concrete properties on resistance to hard projectile impact, ACI Struct. J. 96(2) (1999) 259-267.

[50] A. Dancygier, D. Yankelevsky, High strength concrete response to hard projectile impact, Int. J. Impact Eng. 18(6) (1996) 583-599.

[51] A.N. Dancygier, D.Z. Yankelevsky, C. Jaegermann, Response of high performance concrete plates to impact of non-deforming projectiles, Int. J. Impact Eng. 34(11) (2007) 1768-1779.

[52] H. Li, W. Chen, H. Hao, Factors influencing impact force profile and measurement accuracy in drop weight impact tests, Int. J. Impact Eng. (2020) 103688.

[53] S. Mindess, N. Banthia, C. Yan, The Fracture-Toughness of Concrete under Impact Loading, Cem. Concr. Res. 17(2) (1987) 231-241.

[54] J.K. Wight, Reinforced Concrete: Mechanics and Design (Seventh Edition), 7th ed., Pearson Education, Inc., New Jersey, USA, 2015.

[55] fib. Bulletin 40, FRP reinforcement in RC structures, International Federation for Structural Concrete (fib), Lausanne, Switzerland, 2007.

[56] T.T. Tran, T.M. Pham, Z. Huang, W. Chen, H. Hao, M. Elchalakani, Impact Response of Fibre Reinforced Geopolymer Concrete Beams with BFRP Bars and Stirrups, (under review) (2020).

[57] C. Zanuy, G.S. Ulzurrun, Residual behavior of reinforced steel fiber‐reinforced concrete beams damaged by impact, Struct. Concr. 20(2) (2019) 597-613.

[58] LSTC, LS-DYNA Theory Manual, Livermore Software Technology Corporation, Livermore, California, USA, 2019.

[59] W.S. Chen, H. Hao, S.Y. Chen, Numerical analysis of prestressed reinforced concrete beam subjected to blast loading, Mater. Des. 65 (2015) 662-674.

[60] Y. Hao, H. Hao, Influence of the concrete DIF model on the numerical predictions of RC wall responses to blast loadings, Eng. Struct. 73 (2014) 24-38.

[61] W. Chen, H. Hao, M. Jong, J. Cui, Y. Shi, L. Chen, T.M. Pham, Quasi-static and dynamic tensile properties of basalt fibre reinforced polymer, Compos Part B-Eng 125 (2017) 123-133.

[62] L.J. Malvar, Review of static and dynamic properties of steel reinforcing bars, ACI Mater. J. 95(5) (1998) 609-616.